World Academy of Science, Engineering and Technology
International Journal of Structural and Construction Engineering
Vol:15, No:12, 2021

Seismic Behavior and Loss Assessment of High-Rise Buildings with Light Gauge Steel-Concrete Hybrid Structure

Bing Lu, Shuang Li, Hongyuan Zhou

***Abstract*—**The steel-concrete hybrid structure has been extensively employed in high-rise buildings and super high-rise buildings. The light gauge steel-concrete hybrid structure, including light gauge steel structure and concrete hybrid structure, is a type of steel-concrete hybrid structure, which possesses some advantages of light gauge steel structure and concrete hybrid structure. The seismic behavior and loss assessment of three high-rise buildings with three different concrete hybrid structures were investigated through finite element software. The three concrete hybrid structures are reinforced concrete column-steel beam (RC-S) hybrid structure, concrete-filled steel tube column-steel beam (CFST-S) hybrid structure, and tubed concrete column-steel beam (TC-S) hybrid structure. The nonlinear time-history analysis of three high-rise buildings under 80 earthquakes was carried out. After simulation, it indicated that the seismic performances of three high-rise buildings were superior. Under extremely rare earthquakes, the maximum inter-story drifts of three high-rise buildings are significantly lower than 1/50. The inter-story drift and floor acceleration of high-rise building with CFST-S hybrid structure were bigger than those of high-rise buildings with RC-S hybrid structure, and smaller than those of high-rise building with TC-S hybrid structure. Then, based on the time-history analysis results, the post-earthquake repair cost ratio and repair time of three high-rise buildings were predicted through an economic performance analysis method proposed in FEMA-P58 report. Under frequent earthquakes, basic earthquakes and rare earthquakes, the repair cost ratio and repair time of three high-rise buildings were less than 5% and 15 days, respectively. Under extremely rare earthquakes, the repair cost ratio and repair time of high-rise buildings with TC-S hybrid structure were the most among three high rise buildings. Due to the advantages of CFST-S hybrid structure, it could be extensively employed in high-rise buildings subjected to earthquake excitations.

***Keywords*—**Seismic behavior, loss assessment, light gauge steel, concrete hybrid structure, high-rise building, time-history analysis.

I. Introduction

THE steel-concrete hybrid structure has been extensively adopted in high-rise buildings and super high-rise buildings in China [1], [2]. The steel-concrete hybrid structure combines some advantages of steel structure and concrete structure, such as light weight, high stiffness, good ductility, and short construction period. The traditional steel-concrete hybrid structure includes steel frame-concrete core tube structure, huge composite column-steel frame-concrete core tube structure, and tube-in-tube structure [3]. A new-type steel-concrete hybrid structure, i.e., light gauge steel-concrete hybrid structure, was developed [4]-[6]. In light gauge steel-concrete hybrid structure, the light gauge steel structure is embedded in concrete hybrid structure. The schematic of light gauge steel-concrete structure is shown in Fig. 1.

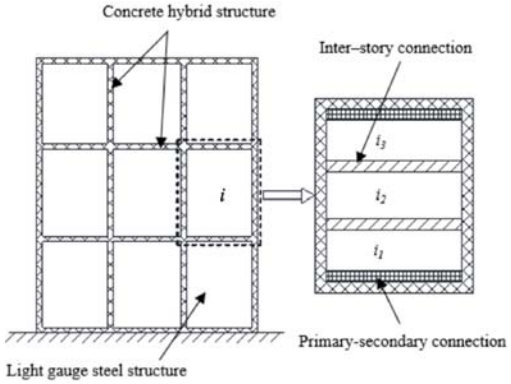

Fig. 1 Light gauge steel-concrete hybrid structure

In recent years, earthquakes happened frequently, the seismic behavior of high-rise buildings has been of interest to researchers. Lei [5] developed an elastic finite element model of high-rise building with light gauge steel-concrete hybrid structure by SAP2000 software. For light gauge steel-concrete hybrid structure, the concrete hybrid structure was primarily used to resist the normal loads and earthquake excitations. It indicated that adding light gauge steel structure could decrease the fundamental period of high-rise building, and the reduction in fundamental period increased with the increases in total height of high-rise building, thickness of wall in light gauge steel structure, and amount of floor in inter-story of concrete hybrid structure. Li et al. [6] performed the experiment to investigate the lateral resistance of light gauge steel-concrete hybrid frame. The experimental results indicated that adding light gauge steel structure could significantly increase the lateral stiffness of concrete hybrid frame. Then, they develop a refined finite element model of high-rise building with light gauge steel-concrete hybrid structure by ABAQUS finite element software. According to the experimental results and simulation results, two formula for calculating the lateral stiffness of light gauge steel structure and predicting the reduction of fundamental period of high-rise building were proposed.

Shuang Li is with Harbin Institute of Technology, China (e-mail: shuangli@hit.edu.cn).

In the researches performed by Lei [5] and Li et al. [6], the concrete hybrid structure in high-rise building was reinforced concrete frame-shear wall structure. As the extensive development of prefabricated structures, the concrete column-steel beam hybrid structure was widely adopted in high-rise buildings due to the convenient construction and superior mechanical performance. Currently, the behavior of three concrete hybrid structures, i.e., reinforced concrete column-steel beam (RC-S) hybrid structure [7]-[9], concrete-filled steel tube column-steel beam (CFST-S) hybrid structure [10]-[12], and tubed concrete column-steel beam (TC-S) hybrid structure [13]-[15], have been investigated. The existing researches on the behavior of three concrete hybrid structures focused on the mechanical performance of components and beam-column joints, but the studies on the seismic response of high-rise buildings with the concrete hybrid structures were rare. In addition, the repair cost and repair time due to the damage of structural and nonstructural components in high-rise building subjected to earthquake excitations have been of significant concern to the owners, occupants, and researchers, which could be analyzed to provide suggestions and solutions for post-earthquake relief and reconstruction of high-rise buildings [16]. An economic performance analysis method was proposed by the Federal Emergency Management Agency (FEMA) in FEMA-P58 report [17]-[19]. The method has been widely employed to evaluate the repair loss and repair time of buildings subjected to earthquake excitations [20]-[24].

In this paper, a proposed high-rise building in Shenzhen city was adopted to study the seismic behavior and loss assessment of high-rise building with light gauge steel-concrete hybrid structure, and the influence of concrete hybrid structure type on the seismic behavior and loss assessment of high-rise building were investigated. Firstly, a finite element model of high-rise building with CFST-S hybrid structure was developed and verified. Then, two other finite element models of high-rise buildings were developed, and the structure type of columns in the two models were replaced by RC-S hybrid structure and TC-S hybrid structure, respectively. Secondly, the seismic response of three high-rise buildings subjected to 40 natural earthquake excitations and 40 artificial earthquake excitations were analyzed, including inter-story drift and floor acceleration. Finally, based on the simulation results and the economic performance analysis method proposed in FEMA-P58 report, the repair cost and repair time of three high-rise buildings under earthquake excitations were calculated and compared.

II. Overview of High-Rise Building

A. Concrete Hybrid Structure

The height of high-rise building is 109.8 m. The concrete hybrid structure contains 12 stories. The first story is podium structure and 5.1 m high; the second story is overhead structure and 4.8 m high; the stories above the second story are uniform and 10 m high. The basement has two stories, and the height of inter-story was 3.8 m. The structural plan layout of first story and the 3D view of concrete hybrid structure in high-rise building are shown in Figs. 2 (a) and (b).

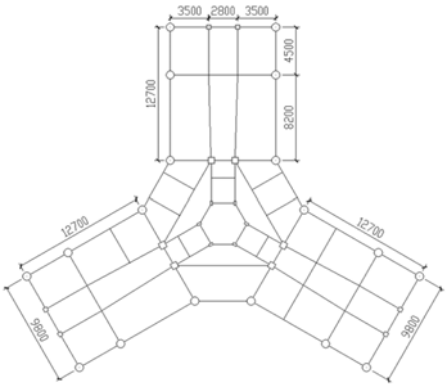

(a) Plan layout of first story

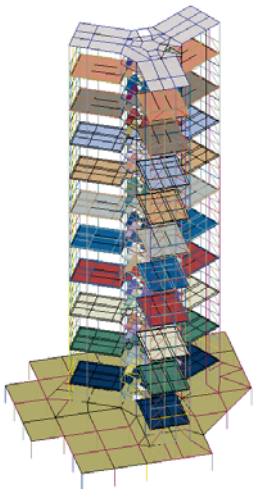

(b) 3D view of concrete hybrid structure

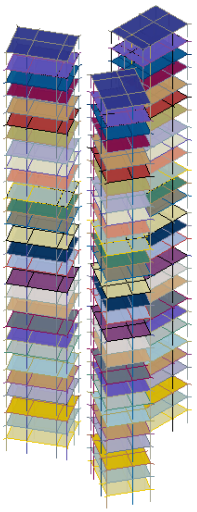

(c) 3D view of light gauge steel structure

Fig. 2 Plan layout of first story and 3D view of concrete hybrid structure and light gauge steel structure in high-rise building

The concrete hybrid structure consists of concrete columns, steel beams, and brace. Three concrete hybrid structures, i.e., RC-S hybrid structure, CFST-S hybrid structure, and TC-S hybrid structure, were employed in three high-rise buildings,

respectively. According to Code for Seismic Design of Buildings (GB 50011-2010) [25], Technical Specification for Concrete Structures of Tall Buildings (JGJ 3-2010) [26], and Technical Specification for Steel Structures of Tall Buildings (JGJ 99-2015) [27], all the components were designed and determined through PKPM software. All the steel beams in three concrete hybrid structures are the same, and they are H-steel beam, Q345 grade. The minimum section of H-steel beam is H550×200×10×14 mm, and the maximum section is H800×300×16×35 mm. The columns in three concrete hybrid structures are different, and the schematic of beam-column joints of three concrete hybrid structures are shown in Figs. 3 (a)-(c). The section of columns in three concrete hybrid structures are designed according to the assumption that the axial strength of columns at the same location were equal. After calculation, the sections of three kinds of columns at different stories are shown in Table I. Fi represents the ith story. In addition, the columns and beams in podium story are reinforced concrete structure, and they are also the same in three concrete hybrid structures. The concrete grade in concrete hybrid columns, RC columns and RC beams is C40, the grade of rebars in RC columns and RC beams is HRB400.

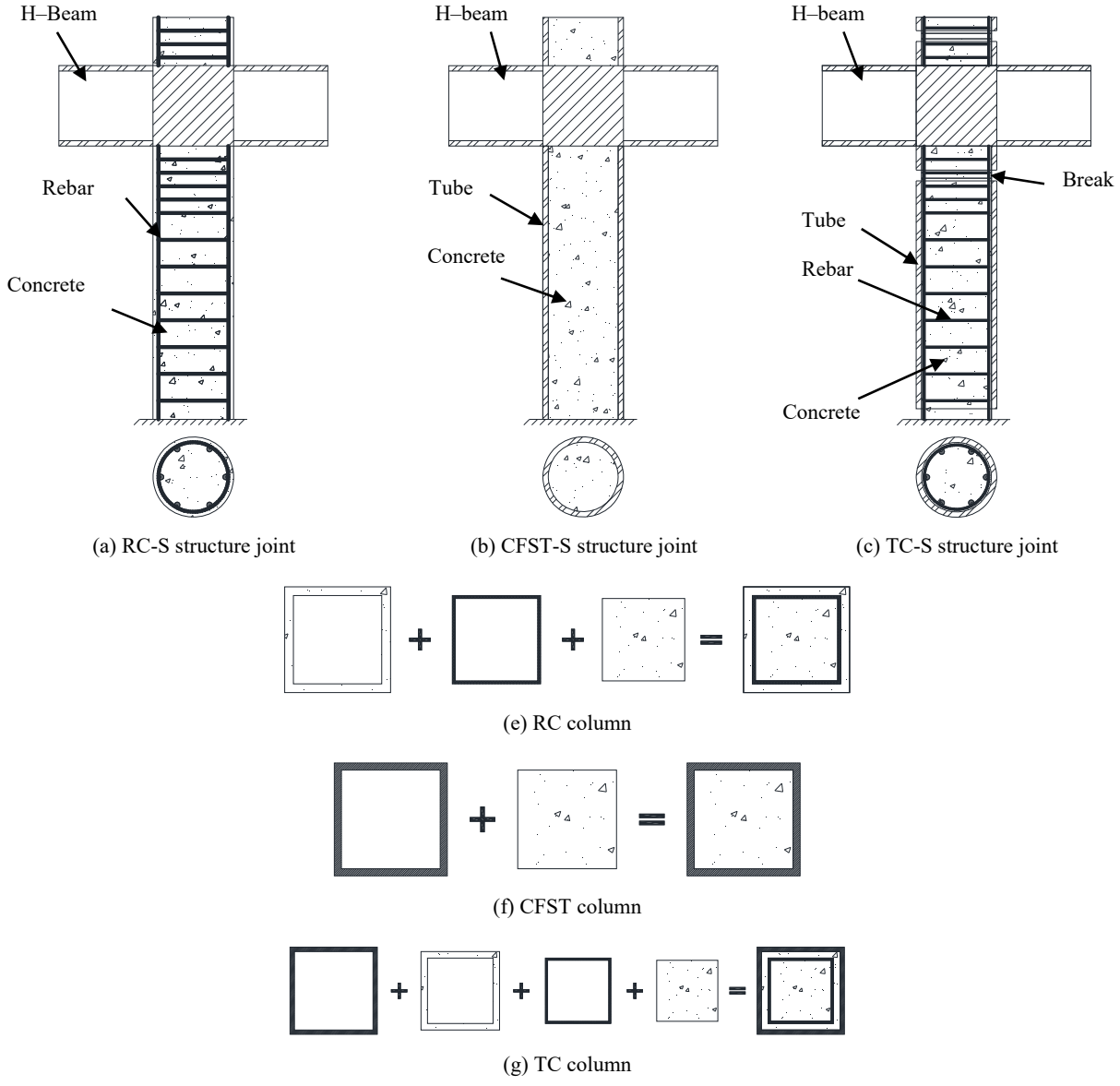

(a) RC-S structure joint (b) CFST-S structure joint (c) TC-S structure joint

(e) RC column

(f) CFST column

(g) TC column

Fig. 3 Schematic of RC-S hybrid structure, CFST-S hybrid structure, and TC-S hybrid structure

The thickness of reinforced concrete slab in podium story is 180 mm, and the thickness of reinforced concrete slab in the other stories is 150 mm. The concrete grade in reinforced concrete slab is C30, and the grade of rebars in slab is HPR300. For stiffening the lateral resisting system of high-rise building, the square steel tube was adopted as brace. The section of brace is 150×150×10×10 mm, and the steel grade is Q345B.

B. Light Gauge Steel Structure

Each story in concrete hybrid structure is divided into three

stories by light gauge steel structure. All the beams and columns are H-steel, and the grade of H-steel is Q345B. The minimum section of H-steel beam is H150×50×6×8 mm, and the maximum section is H400×200×8×14 mm. The outer H-steel column is H300×200×14×14 mm, and the inner H-steel column is H300×200×16×16 mm. The thickness of reinforced concrete slab in light gauge steel structure is 120 mm, and the grade of concrete in the slab is C30, and the grade of rebars in the slab is HPB300. The front view and 3D view of light gauge steel structure are shown in Fig. 2 (c).

III. Finite Element Model of High-Rise Building

A. Element

ABAQUS finite element software was used to develop three finite element models of high-rise buildings with different concrete hybrid structures. Three element types are employed in the finite element model: the shell element, the beam element, and the multi-beam element. The S4R shell element is used to simulate the behavior of slab, and the rebar layer is adopted to simulate the behavior of longitudinal and transversal rebars in slab. The width of shell element is 0.8 m~1.2 m. The B31 beam element is used to simulate the behavior of H-steel column, H-steel beam, and brace, and the length of beam element is 0.8 m~1.2 m.

In this paper, the multi-beam element is used to simulate the behavior of RC column, RC beam, CFST column, and TC column. The multi-beam element consists of some beam elements, and the beam elements were tied each other. Yu et al. [28] simulate the behavior of CFST column by multi-beam element. Considering effects of section shape and hollow ratio, the hysteretic constitutive model of confined concrete and some key parameters were also proposed. After simulation, the experimental results verified the accuracy and rationality of simulation method using multi-beam element.

For RC column and RC beam, three B31 beam elements are adopted to simulate cover concrete, longitudinal rebars, and confined concrete, respectively. For CFST column, two B31 beam elements are used to simulate tube and confined concrete, respectively. For TC column, four B31 beam elements are used to simulate tube, cover concrete, longitudinal rebars, and confined concrete, respectively. The schematics of three columns are shown in Figs. 3 (d)-(f).

B. Material

The kinematic hardening plasticity constitutive model considering Bauschinger effect is used to simulate the behavior of H-steel beam, H-steel column, and rebars. The stress-strain relationship of steel is assumed bilinear. For steel, the elastic modulus of steel (E_s) is 2.06×10^5 MPa, and the hardening modulus (b) of steel is 0.01 times the elastic modulus, and the ultimate strength is 1.4 times the yield strength. For HRB400, the yield strength is 400 MPa, and the ultimate strength is 560 MPa. For HRB300, the yield strength is 300 MPa, and the ultimate strength is 420 MPa. For Q345B, the yield strength is 345 MPa, and the ultimate strength is 483 MPa.

The concrete damage plasticity constitutive model is used to simulate the behavior of plain concrete, such as the cover of reinforce concrete beam and reinforced concrete column as well as slab. The compressive stress-strain relationship of plain concrete is developed according to the relationship proposed by Careira and Chu [29], as shown in the following:

$$\sigma_{co} = \frac{f_c \beta (\varepsilon_{co}/\varepsilon_c)}{\beta - 1 + (\varepsilon_{co}/\varepsilon_c)^{\beta}} \tag{1}$$

$$\beta = \frac{\varepsilon_{co}/\varepsilon_c}{1 - f_c/(\varepsilon_{co}/\varepsilon_c)} \tag{2}$$

where, σ_{co} is the compressive stress of concrete, ε_{co} is the compressive strain of concrete, f_c is the compressive strength of concrete cylinder, ε_c is the strain corresponding to f_c, which is taken as 0.002. β is a function of secant modulus of elasticity. Other plasticity parameters including dilation angel of 30°, flow potential eccentricity of 0.667, the ratio of the biaxial compressive strength to uniaxial compressive strength that is equal to 1.16, and eccentricity of 0.1 were set for the concrete damage plasticity model.

The tension stress-strain relationship of plain concrete is based on the stress-fracture energy cracking model, and the fracture energy parameter was calculated based on an equation stipulated in CEB-FIP [30], as shown in the following:

$$G_f = a_f (f_c/10)^{0.7} \tag{3}$$

where G_f is the fracture energy, and a_f is a coefficient related to the maximum size of coarse aggregate, taken as 0.3 here. The concrete damage plasticity model has two failure mechanisms, including tensile cracking and compressive crushing. These two failure mechanisms were associated with two damage variables, d_t and d_c, which characterize the degradation of E_c. Birtel and Mark [31] proposed the evolution law of d_c that was associated with concrete plastic strain $\varepsilon_{p,c}$ that was proportional to the concrete inelastic strain through a constant factor b_c. The evolution law is shown in the following:

$$d_c = 1 - \frac{\sigma_{co} E_c^{-1}}{\varepsilon_{p,c}(1/b_c - 1) + \sigma_{co} E_c^{-1}} \tag{4}$$

According to the comparison between experimental results and simulation result, Birtel et al. conjectured that the b_c could be assumed as 0.7, which was adopted in this model. The d_t could be calculated based on (5) proposed by Gopalaratnam and Shahcrack [32], in which the degradation of E_c is equal to the ratio of the reduction in tensile strength (σ_{to}) to the peak tensile strength (f_t):

$$d_t = 1 - \frac{\sigma_{to}}{f_t} \tag{5}$$

For plain concrete, E_c, f_c, and f_t could be determined according to the Code for Design of Concrete Structures (GB

50010-2010) [33].

The stress-strain relationship of steel tube in CFST column and TC column is simulated by the Giuffre-Menegotto-Pinto (G-MP) constitutive model considering Bauschinger effect [34]. Ten parameters in G-MP constitutive model should be determined, including yield strength (f_y), elastic modulus (E_s), the ratio (b) between hardening modulus and elastic modulus, the control parameter (R_0), coefficients RC_1, RC_2, A_1, A_2, A_3, and A_4. Except for f_y, E_s, and b, the other seven parameters for different grade steel are assumed as the same due to the absence of experimental results, and they are 20, 0.925, 0.15, 0, 1, 0, 1, respectively.

The stress-strain relationship of confined concrete in RC column, RC beam, CFST column, and TC column is simulated by the modified Kent-Park model proposed by Scott et al. [35]. According to the researches carried out by Yu et al. [36], the formula for calculating the axial capacity of CFST column could be shown as:

$$\mathrm{N}_{sc} = (1+0.5k_e\frac{\xi}{1+\xi})\left[A_c f_c + A_s f_y\right] = (1+0.5k_e\xi)A_c f_c + A_s f_y \tag{6}$$

$$\xi = A_s f_y / A_c f_c \tag{7}$$

$$k_e = (n^2-4)/(n^2+20) \tag{8}$$

where $\mathrm{N_{sc}}$ is the axial capacity of CFST column, A_c is the area of concrete, A_s is the area of steel tube, ξ is confining coefficient, k_e is confinement effectiveness coefficient, n is the side number, for circular tube, $n \approx \infty$.

$$\mathrm{N}_{sc} = A_c f_{cc} + A_s f_y \tag{9}$$

$$f_{cc} = Kf_c, \quad K = 1+0.5k_e\,\xi \tag{10}$$

$$\varepsilon_{cc} = K\varepsilon_c \tag{11}$$

where f_{cc} is the ultimate strength of confined concrete, ε_{cc} is the strain corresponding to f_{cc}.

The maximum strain of confined concrete (ε_{cu}) and the stress corresponding to ε_{cu} (f_{cu}) could be calculated by:

$$\left.\begin{aligned}\varepsilon_{cu} &= k\varepsilon_{cc}\\ f_{cu} &= \alpha f_{cc}\end{aligned}\right\} \tag{12}$$

where k and α are coefficients. According to Mander constitutive model [37], f_{cu} could be calculated by:

$$f_{cu} = \frac{x_u r}{r-1+x_u^r} f_{cc} \tag{13}$$

$$x_u = \varepsilon_{cu}/\varepsilon_{cc} = k \tag{14}$$

$$\alpha = \frac{kr}{r-1+k^r} \tag{15}$$

$$\chi = \frac{0.09k\sqrt{k}+\alpha/2}{0.09k\sqrt{k}+1} \tag{16}$$

where r is curve shape coefficient, χ damage coefficient of modulus. According to research carried out by Yu et al. [36], r = 2/K, k = 5. The tensile strength (f_t) and tensile modulus (E_t) could be calculated by:

$$f_t = f_c/10, \quad E_t = E_c/10 \tag{17}$$

In the finite element model of high-rise building, the G-MP constitutive model and modified Kent-Park constitutive model were developed by using ABAQUS user-defined material subroutines.

C. Verification of Finite Element Model of High-Rise Building

For ensuring the accuracy of finite element model of high-rise building by using ABAQUS finite element software, YJK finite element software was used to develop another finite element model of the same high-rise building. The natural vibration period, the modal assurance criterion (MAC), and the seismic response of two high-rise buildings with CFST-S hybrid structure using ABAQUS software and YJK software were compared.

The first 10 natural vibration periods of the high-rise building using ABAQUS software are 3.497 s, 3.460 s, 2.681 s, 1.062 s, 1.041 s, 0.822 s, 0.567 s, 0.561 s, 0.468 s, and 0.401 s. The first 10 natural vibration periods of the high-rise building using ABAQUS software are 3.571 s, 3.559 s, 2.618 s, 1.081 s, 1.071 s, 0.781 s, 0.581 s, 0.570 s, 0.410 s, and 0.390 s. The differences of natural vibration periods between two high-rise buildings are little, less than 5.1%. The MAC was proposed by West, which was used to compare the uniformity of two finite element models [38]. The formula for calculating MAC is shown in the following:

$$MAC\left(\varphi_i,\varphi_j\right) = \frac{\left|\varphi_i^T\varphi_j\right|^2}{\varphi_i^T\varphi_i\varphi_j^T\varphi_j} \tag{18}$$

where φ_i *and* φ_j are the i modal vector of one model and j modal vector of the other model, respectively. After calculating, for the first three modals, the MACs of two high-rise buildings were 0.9997, 0.9997 and 0.9986, which means that the difference between two models could be negligible.

The seismic response of two high-rise buildings were investigated and compared. As shown in Fig. 4, Fig. 4 (a) is the earthquake excitation, Chalfant Valley-02 Long Valley Dam, and Fig. 4 (b) is the relative displacement of top point in two high-rise buildings subjected to earthquake excitation. The relative displacement-time curve of high-rise building using ABAQUS software is similar to that using YJK software. Thus, according to the natural vibration period, the MAC, and the

relative displacement-time curves, the accuracy of finite element model of high-rise building using ABAQUS software could be verified.

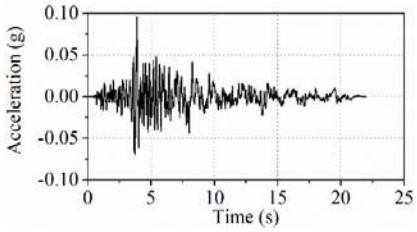

(a) Ground motion

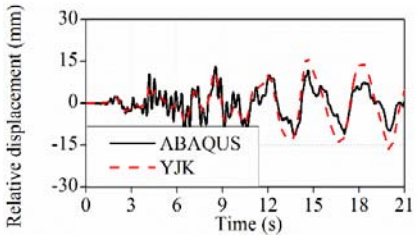

(b) Relative displacement

Fig. 4 Time-history analysis

D. Basic Dynamic Properties of Three High-Rise Buildings

The modal analysis of three high-rise buildings were carried out, and the first 10 natural vibration periods of three high-rise buildings were calculated. The first 10 natural vibration periods of the high-rise building with RC-S structure are 3.536 s, 3.534s, 2.731s, 1.079s, 1.076s, 0.861s, 0.593s, 0.591s, 0.485s, and 0.426s. The first 10 natural vibration periods of the high-rise building with TC-S structure are 3.671 s, 3.667 s, 2.845 s, 1.098 s, 1.095 s, 0.863 s, 0.602 s, 0.596 s, 0.487 s, and 0.428 s. The fundamental period of three high-rise buildings is about 3.53 s. For high-rise building with RC-S hybrid structure, the natural vibration periods are slightly higher than those with CFST-S hybrid structure, and slightly lower than those with TC-S hybrid structure. The differences of natural vibration periods among three high-rise buildings are little, which indicated that the stiffness of three high-rise buildings is similar.

IV. Seismic Behavior of High-Rise Building

A. Selection and Modification of Earthquake Records

The seismic responses of three high-rise buildings under frequent earthquakes, basic earthquakes, rare earthquakes, and extremely rare earthquakes were simulated. The peak ground accelerations (PGA) of frequent earthquakes, basic earthquakes, rare earthquakes, and extremely rare earthquakes are 0.035 g, 0.1 g, 0.22 g, and 0.3 g, representing an earthquake event with 50 year, 475 year, 2,000 year, and 10,000 year return period, respectively. For each different intensity earthquakes, 10 earthquake records were selected from PEER-NGA-Records, and the other 10 earthquake records were developed using SIMQKE-GR software. It is stipulated in GB 50011-2010 [25] that the differences between the selected earthquake spectrum and designed earthquake spectrum should be less than 20%. The response spectrum of the adopted records and design spectrum are shown in Fig. 5. After comparison, it indicates that the selected earthquake records satisfy the stipulations in GB 50011-2010 [25].

B. Inter-Story Drift

The time-history analysis of three high-rise buildings under 80 earthquake records were performed by using ABAQUS finite element software. For example, the inter-story drifts of high-rise building with CFST-S hybrid structure along X direction under basic earthquakes, and rare earthquakes, and extremely rare earthquakes are shown in Figs. 6 (a)-(c). Under frequent earthquakes, the X-inter-story drifts of all stories in high-rise building are lower than 1/300, which is the maximum inter-story drift of building under elastic stage stipulated in technical code for concrete filled steel tubular structures (GB 50936-2014) [39].

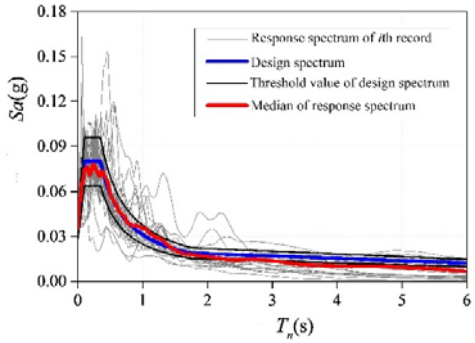

(a) Frequent earthquake (PGA = 0.035g)

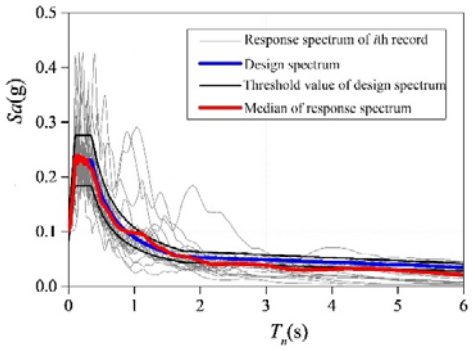

(b) Basic earthquake (PGA = 0.1g)

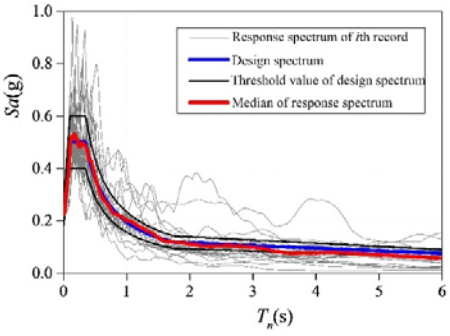

(c) Rare earthquake (PGA = 0.22g)

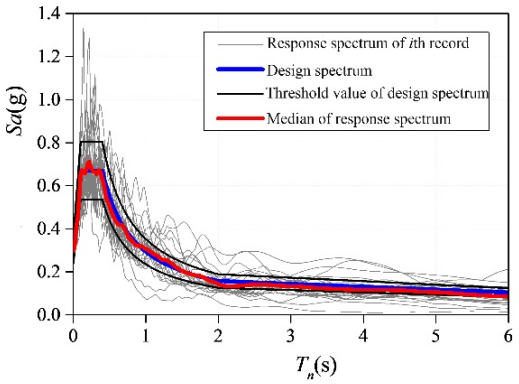

(d) Extreme rare earthquake (PGA = 0.3g)

Fig. 5 Comparison of response spectrum and design spectrum

Under a few of basic earthquakes and most of rare earthquakes, the X-inter-story drifts of high-rise building are higher than 1/300. Under extremely rare earthquake, the X-inter-story drifts of all stories in three high-rise building are lower than 1/50, which is the maximum inter-story drift of building under plastic stage stipulated in GB 50936-2014 [39]. The inter-story drift curves are zigzag, which is due to the abruptness of lateral stiffness in high-rise building. The inter-story drifts of top stories and bottom stories are lower than those of middle stories. The X-inter-story drift of three high-rise buildings were similar.

The mean and maximum of X-inter-story drift and Y-inter-story drift of three high-rise buildings were calculated and shown in Figs. 7 (a)-(d), respectively. It indicates that the X-inter-story drifts are higher than Y-inter-story drifts. The inter-story drift increases with the increase in PGA. The inter-story drifts of high-rise building with RC-S hybrid structure are lower than those of high-rise buildings with CFST-S hybrid structure and TC-S hybrid structure. The difference of mean inter-story drifts between CFST-S hybrid structure and TC-S hybrid structure are small, and the maximum inter-story drifts of TC-S hybrid structure are higher than those of CFST-S hybrid structure.

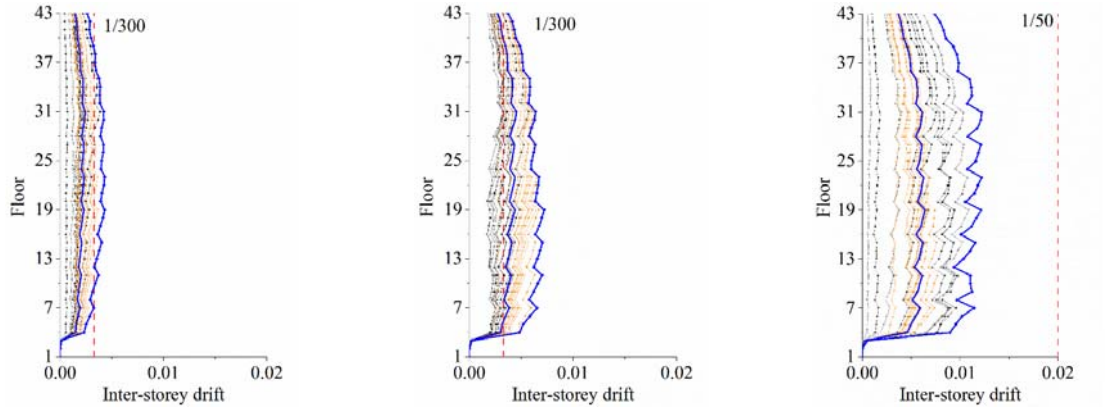

(a) Under basic earthquake (b) Under rare earthquake (c) Under extremely rare earthquake

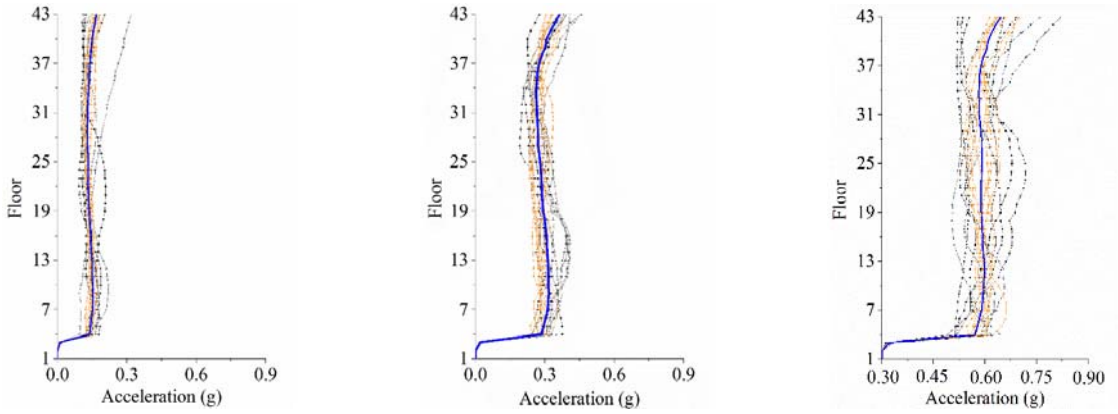

(e) Under basic earthquake (f) Under rare earthquake (g) Under extremely rare earthquake

Fig. 6 X-inter-story drifts and X-floor accelerations of high-rise building with CFST-S hybrid structure

C. Floor Acceleration

The floor acceleration of high-rise building with CFST-S hybrid structure along X direction under basic earthquakes, rare earthquakes, and extremely rare earthquakes are shown in Figs. 6 (d)-(f). It is shown that the X-floor acceleration of most stories in high-rise building are about 0.15 g, 0.3 g and 0.6 g, respectively, which are significantly larger than the corresponding PGAs. The floor accelerations of top stories are

larger than those of middle stories and the bottom stories. The X-floor accelerations of three high-rise buildings were similar.

The mean and maximum of X-floor acceleration and Y-floor acceleration of three high-rise buildings were calculated and shown in Figs. 7 (e)-(h), respectively. It indicates that the X-floor-accelerations are higher than Y-floor-accelerations, and the floor acceleration increases with the increase in PGA. The maximum X-floor-acceleration of high-rise building with RC-S hybrid structure are lower than those with CFST-S hybrid structure and TC-S hybrid structure. Except for maximum X-floor-acceleration, the differences of floor acceleration among three high-rise buildings are negligible.

V. Loss Assessment of High-Rise Building under Earthquake

The FEMA P-58 method was used to evaluate the repair cost and repair time of three high-rise buildings subjected to earthquake excitations. The FEMA P-58 method includes three steps: 1) Developing performance model of building; 2) Performing time-history analysis and proposing engineering demand parameters (EDP); 3) Assessing loss. The first step is to collect the basic information of building, such as story number, story height, building area and so on. Meanwhile, all the performance groups of building should be developed. For each performance group, the vulnerability of structural components and nonstructural components could be determined by the same EDP. About 700 performance groups were proposed in FEMA P-58 report, and the vulnerability curves and result functions of every performance group are also developed. In FEMA P-58 report, every performance group has been numbered. According to the basic information of high-rise building in this paper, the number of performance groups of the high-rise building could be selected, and the corresponding vulnerability curves and result functions could be employed. Table II shows the performance groups in the high-rise building with CFST-S hybrid structure.

The mean of inter-story drift (ISD) and mean of peak floor acceleration (PFA) were employed as EDP in this paper. The FEMA P-58 method is based on Monte Carlo algorithm, so the loss assessment is determined stochastically. Each calculation is called one realization. In this paper, the PACT software was used to calculate the repair cost and repair time of three high-rise buildings. The basic information of building, performance groups, and EDP of components calculated in time-history analysis were input to PACT software. A total of 500 realizations were carried out, and the exceeding probability curve of repair cost and repair time of high-rise buildings under different intensity earthquakes were calculated. The total cost of high-rise buildings was various for different cities, different countries, and different time, so the repair cost ratio between repair cost and total cost was used to compare the difference of repair cost among three high-rise buildings, which could eliminate the influence of city, country, and time. The repair cost ratio and repair time with 50% exceeding probability are regarded as reference value.

TABLE I
Section of Columns in Three High-Rise Buildings

High-rise building	Type	Number	Section (mm)		
			F1-F11	F12-F20	F21-Top
CFST-S structure	Circular	GKZ1	P800x18	P800x14	P800x12
		GKZ1a	P800x14	P800x12	P800x10
		GKZ1b	P800x18	P800x12	P800x12
	Rectangular	GKZ2	□350x600x14x20		
		GKZ3	□600x250x22x16	□600x250x20x16	
RC-S structure	Circular	GKZ1	Φ1200	Φ1190	
		GKZ1a	Φ1160	Φ1150	
		GKZ1b	Φ1200	Φ1150	
	Rectangular	GKZ2	□1000x500		
		GKZ3	□1000x440	□1000x400	
TC-S structure	Circular	GKZ1	P770x18	P770x14	
		GKZ1a	P770x14	P770x12	
		GKZ1b	P770x18	P770x12	
	Rectangular	GKZ2	□320x560x18x20		
		GKZ3	□220x560x20x18	□560x180x20x18	

As shown in Fig. 8, the repair cost ratios and repair times of three high-rise buildings with three concrete hybrid structures increase with the increase in PGA. Under frequent and basic earthquakes, the repair cost ratio and repair time of three high-rise buildings are negligible, and the structural components are intact. Under rare earthquakes, only a few structural components of high-rise building with TC-S hybrid structure fractured, and the repair cost ratios of three high-rise buildings are less than 5%. Under extremely rare earthquakes, the repair cost ratio of structural components of high-rise building with TC-S structure is the highest among three high-rise buildings, which reaches 30%. The repair cost ratios of the other two high-rise buildings are about 18%. Under frequent and basic earthquakes, the repair time of each high-rise buildings is less than five days, and the differences among three high-rise buildings are negligible. Under rare earthquake, the repair time of each high-rise building is less than 16 days, and the difference between high-rise building with TC-S hybrid structure and high-rise building with RC-S hybrid structure is about five days. Under extremely rare earthquake, the repair time of high-rise building with RC-S hybrid structure is the lowest, which is 105 days. The repair time of high-rise building with TC-S hybrid structure reaches 150 days, which is higher than that of high-rise building with CFST-S hybrid structure by 15 days.

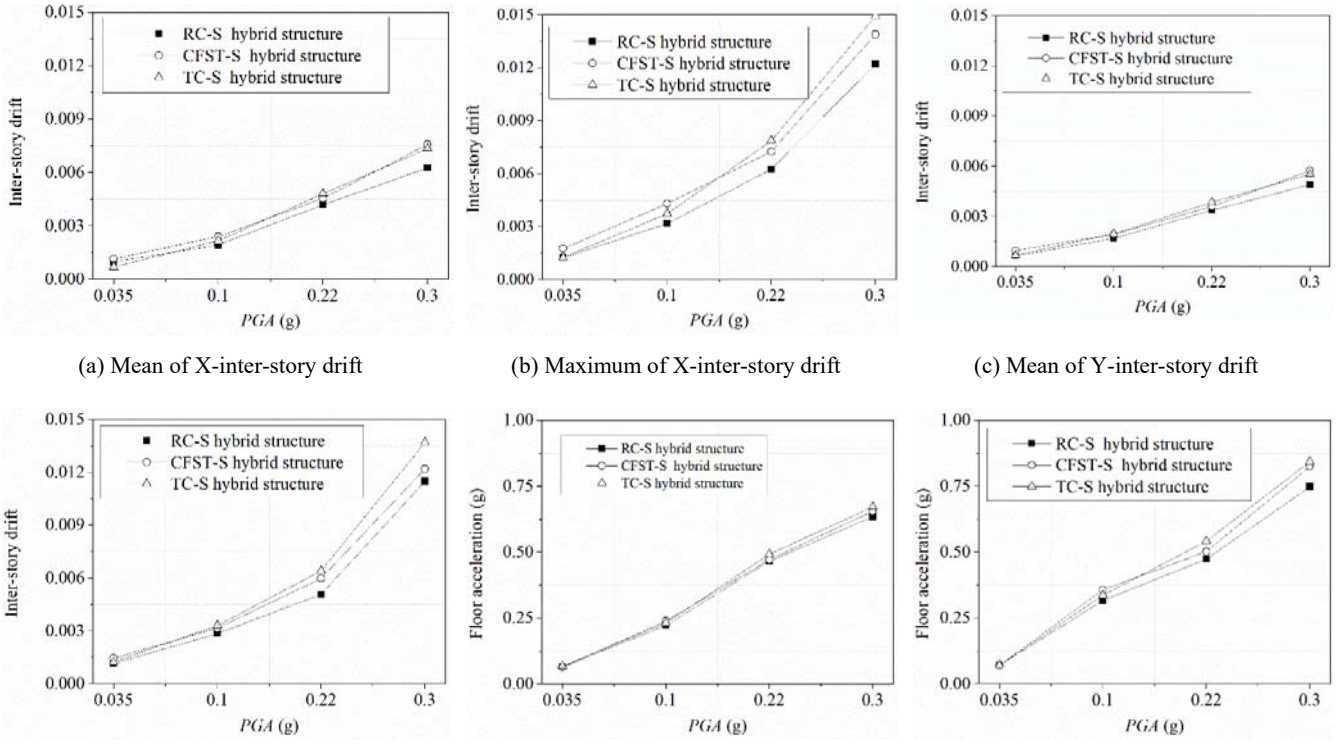

(a) Mean of X-inter-story drift (b) Maximum of X-inter-story drift (c) Mean of Y-inter-story drift

(d) Maximum of Y-inter-story drift (e) Mean of X-floor acceleration (f) Maximum of X-floor acceleration

(g) Mean of Y-floor acceleration (h) Maximum of Y-floor acceleration

Fig. 7 Mean and maximum of inter-story drifts and floor accelerations of three high-rise buildings

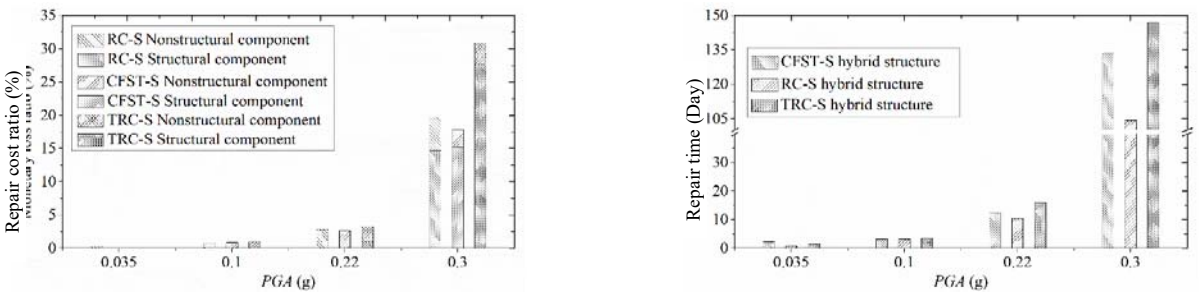

a) Repair cost b) Repair time

Fig. 8 Loss assessment of high–rise building

VI. Conclusion

This paper investigates the seismic performance and loss assessment of three high-rise buildings with three concrete hybrid structures under 80 earthquakes. The inter-story drifts and floor accelerations of three high-rise buildings were simulated, and the repair cost ratio and repair time were compared and analyzed. The differences of inter-story drift among three high-rise buildings are little. Meanwhile, the

differences of floor acceleration among three high-rise buildings are also negligible. It indicated that the seismic performance of RC-S hybrid structure, CFST-S hybrid structure, and TC-S hybrid structure are similar. The CFST-S hybrid structure and TC-S hybrid structure have some advantages over RC-S hybrid structure, such as convenient construction and short construction period. Due to the advantages of CFST-S hybrid structure, it could be extensively employed in high-rise buildings subjected to earthquake excitations.

TABLE II
INFORMATION OF PERFORMANCE GROUPS IN HIGH-RISE BUILDING WITH CFST-S HYBRID STRUCTURE

Performance group		Number	Unit price ($)	Unit	Total	EDP
Structural component	Unilateral RC-RC	B1041.043a	—	Single	5	ISD
	Bilateral RC-RC	B1041.043b	—		21	ISD
	Unilateral CFST-S	B1041.043a	—	Single	564	ISD
	Bilateral CFST-S	B1041.043b	—		126	ISD
	S-S1	B1035.032	—	Single	402	ISD
	S-S2	B1035.051	—	Single	1140	ISD
	Slab column connection	B1049.031	—	Single	525	ISD
	Brace	B1033.111c	—	Single	360	ISD
	Exterior wall	B2011.201a	—	30SF	4161	ISD
	Partition wall	C1011.001a	—	100LF	106.5	ISD
Nonstructural component	Lamp	C3034.002	3.6	Single	549	PFA
	Television	E2022.021	476.2	Single	168	PFA
	bed	E2022.020	317.5	Single	168	PFA
	Tables and chairs	E2022.020a	234.9	Set	84	PFA
	Kitchen equipment	E2022.020b	1269.8	Set	84	PFA
	Toilet equipment	E2022.020c	952.4	Set	174	PFA
	Elevator	D1014.011	—	Single	2	PFA
	Roof	B3011.011	—	100LF	462	PFA
	Hot water pipe	D2022.011a	—	1000LF	0.71	PFA
		D2022.021a	—	1000LF	0.71	PFA
	Cold water pipe	D2021.011a	—	1000LF	2.14	PFA
	HVAC pipeline	D3041.011a	—	1000LF	7.14	PFA
	Sewage pipe	D2031.011b	—	1000LF	17.52	PFA
	Fire sprinkler	D4011.031a	—	100EA	17.14	PFA
	VAV equipment	D3041.041a	—	10EA	57.48	PFA

Note: 1. LF represents feet, SF represents square feet, EA represents single; 2. A-B represents column type-beam type; 3. "—" represents the value determined according to the database in PACT software.

ACKNOWLEDGMENT

This research project was funded by the National Key R&D Program of China (grant number 2016YFC0701500).

REFERENCES

[1] H. J. Jiang, B. Fu, L. E. Liu, X. W. Yin, "Study on seismic performance of a super-tall steel-concrete hybrid structure," *The Structural Design of Tall and Special Buildings*, vol. 23(5), pp. 334-349, Aug 2012.
[2] Z. X. Li, Y. Lv, L. H. Xu, Y. Ding, Q. Zhao, "Experimental studies on nonlinear seismic control of a steel-concrete hybrid structure using MR dampers," *Engineering Structures*, vol. 49, pp. 248-263, Apr, 2013.
[3] D. R. Wang, J. Zhou, "Development and prospect of hybrid high-rise building structures in China," *Journal of Building Structures*, vol. 31(6), pp.28-32, June 2010.
[4] L. Z. Han, *The elastic-plastic analysis on the light steel and concrete high-rise mixed structure*, Chongqing City, Chongqing University, 2016.
[5] Y. Lei, *Calculating on Period and Seismic of Light-steel and concrete high-rise mixed structure*, Chongqing City, Chongqing University, 2012.
[6] Q. Li, Z. J. Wang, Y. C. Deng, L. Z. Han, "Study on the period reduction factor of Light gauge steel-concrete mixed structure," *Journal of Civil and Environment Engineering*, vol. 42(01), pp. 98-107, 2019.
[7] T. M. Sheikh, G. G. Ddeuerlein, J. A. Yura, J. O. Jirsa, "Beam-column moment connections for composite frames: Part 1" *Journal of Structural engineering*, vol. 115(11), pp. 2858-2876, Nov 1989.
[8] X. Liang, G. J. Parra-Monteinos, "Seismic behavior of reinforced concrete column-steel beam subassemblies and frame systems," *Journal of Structural Engineering*, vol. 130(2), pp. 310-319, Jan 2004.
[9] A. Khaloo, R. B. Doost, "Seismic performance of precast RC column to steel beam connections with variable joint configurations," *Engineering Structures*, vol. 160, pp. 408-418, Apr 2018.
[10] J. Beutel, D. Thambiratnam, N. Perera, "Monotonic Behavior of Composite Column to Beam Connections," *Engineering Structures*, vol. 23(9), pp. 1152-1161, Sep 2001.
[11] J. W. Hu, Y. S. Kang, D. H. Choi, T. Park, "Seismic design, performance, and behavior of composite-moment frames with steel beam-to-concrete filled tube column connections," *International Journal of Steel Structures*, vol. 10(2), pp. 177-191, Jun 2010.
[12] M. Z. Jeddi, N. H. R. Sulong, M. M. A. Khanouki, "Seismic performance of a new through rib stiffener beam connection to concrete-filled steel tubular columns: an experimental study," *Engineering Structures*, vol. 131, pp. 477-491, Jan 2017.
[13] Y. Sun, K. Sakino, "Earthquake-resisting Performance of RC Column Confined by Square Steel Tubes: Part 1: Columns under High Axial Load," *Journal of Structural and Constructional Engineering*, vol. 62(501), pp. 93-101, 1997.
[14] S. M. Zhang, J. Liu, L. Ma, T. Xing, "Axial compression test and analysis of circular tube confined HSC stud columns," *China Civil Engineering Journal*, vol. 40(3), pp. 24-31, 2007.
[15] D. Gan, X. H. Zhou, J. P. Liu, B. Yan, "Calculation for shear strength of reinforced-concrete columns constrained by steel tubes," *Journal of Building Structures*, vol. 39, pp. 96-103, 2018.
[16] S. D. Koduru, T. Haukaas, "Probabilistic seismic loss assessment of a Vancouver high-rise building," *Journal of Structural Engineering*, vol. 136(3), pp. 235-245, Sep 2009.

[17] FEMA F 445, Nest-Generation Performance-based seismic design guideline program plan for new and existing buildings, Redwood City: Applied Technology Council, 2006.
[18] FEMA P 58, Seismic performance assessment of buildings Volume 1-Methodology, Washington: Applied Technology Council, 2012a.
[19] FEMA P 58, Sesimic performance assessment of buildings Volume 2-Implementation Guide, Washington: Applied Technology Council, 2012b.
[20] G. M. Del Gobbo, M. S. Williams, A. Blakeborough, "Seismic performance assessment of Eurocode 8-compliant concentric braced frame buildings using FEMA P-58," *Engineering Structures*, vol. 155, pp. 192-208, Jan 2018.
[21] Cremen Gemma, M. Eeri, W. Baker. Jack, "A Methodology for Evaluating Component-Level Loss Predictions of the FEMA P-58 Seismic Performance Assessment Procedure," *Earthquake Spectra*, vol. 35(1), pp. 193-210, Nov 2019.
[22] C. Del Vecchio, M. D. Ludovico, S. Pampanin, A. Prota, "Repair Costs of Existing RC Buildings Damaged by the L'Aquila Earthquake and Comparison with FEMA P-58 Predictions," *Earthquake Spectra*, vol. 34(1), pp. 237-263, Dec 2018.
[23] C. Gemma, J. W. Baker, "Quantifying the Benefits of Building Instruments to FEMA P-58 Rapid Post-Earthquake Damage and Loss Predictions," *Engineering Structures*, vol. 176, pp. 243-253, Dec 2018.
[24] Z. Xu, H. Zhang, X. Lu, Y. Xu, Z. Zhang, Y. Li, "A prediction method of building seismic loss based on BIM and FEMA P-58," *Automation in Construction*, vol. 102, pp. 245-257, Jun 2019.
[25] GB 50011-2010, Code for Seismic Design of Buildings, Beijing: China Architecture & Building Press, 2016.
[26] JGJ 3-2010, Technical Specification for Concrete Structures of Tall Buildings, Beijing: China Architecture & Building Press, 2010.
[27] JGJ 99-2015, Technical Specification for Steel Structures of Tall Buildings, Beijing: China Architecture & Building Press, 2015.
[28] M., Yu, X. X. Cha, "A unified fiber element model for solid and hollow concrete-filled steel tube," *Industrial Construction*, vol. 44(02), pp. 123-129, Apr 2014.
[29] D. J. Carreira, K. H. Chu, "Stress-strain relationship for plain concrete in compression," *Journal of the American Concrete Institute*, vol. 82(6), pp. 797-804, 1985
[30] CEB-FIP, Model Code 2010. Switzerland: Comité Euro-International du Béton, Secretariat Permanent, 2010.
[31] V. Birtel, P. Mark, "Parameterised Finite Element Modelling of RC Beam Shear Failure," *ABAQUS User's Conference*, 2006.
[32] V. S. Gopalaratnam, S. P. Shah, "Softening response of plain concrete in direct tension," *Journal Proceedings*, vol. 82(3), pp. 310-323, 1985.
[33] GB 50010-2010, Code for design of concrete structures, Beijing: China Architecture & Building Press, 2015.
[34] F. Fabio, E. S. Taucer, C. Filippou. Filip, A fiber beam-column element for seismic response analysis of reinforced concrete structures, Earthquake Engineering Research Center College of Engineering University of California, Berkeley, 1991.
[35] B. D. Scott, R. Park, M. J. N. Priestley, "Stress-strain behavior of concrete confined by overlapping hoops at low and high strain rates," *Journal proceedings*, vol 79(1), pp. 13-27, 1982.
[36] M. Yu, X. X. Zha, J. Q. Ye, Y. T, Li, "A unified formulation for circle and polygon concrete-filled steel tube columns under axial compression," *Engineering Structures*, vol. 49(2), pp. 1-10, Apr 2013.
[37] J. B. Mander, M. Priestley, R. Park, "Theoretical stress-strain model for confined concrete," *Journal of Structural Engineering*, vol. 114(8), pp. 23, 1988.
[38] W. M. West, "Illustration of the use of model assurance criterion to detect structural changes in an orbiter test specimen," *Proceedings of the 4th International Modal Analysis Conference*, 1986.
[39] GB 50936-2014, Technical code for concrete filled steel tubular structures, Beijing: China Architecture & Building Press, 2014.